Thermomechanical Response of a Representative Porin for Biomimetics

Lopes Rodrigues, Maximilien; Puiggalí-Jou, Anna; Marti-Balleste, D; del Valle, Luis J; Michaux, Catherine; Perpète, Eric; Alemán, Carlos

Published in:
ACS Omega

DOI:
10.1021/acsomega.8b00463

Publication date:
2018

ACS OMEGA

Article

Cite This: ACS Omega 2018, 3, 7856−7867

Thermomechanical Response of a Representative Porin for Biomimetics

Maximilien Lopes-Rodrigues,[†,‡,§,∥] Anna Puiggalí-Jou,[†,‡,∥] Didac Martí-Balleste,[†,‡] Luis J. del Valle,[†,‡] Catherine Michaux,[§] Eric A. Perpète,[§] and Carlos Alemán*[,†,‡]

[†]Departament d'Enginyeria Química, EEBE, Universitat Politècnica de Catalunya, C/ Eduard Maristany, 10-14, Ed. I2, 08019 Barcelona, Spain

[‡]Barcelona Research Center for Multiscale Science and Engineering, Universitat Politècnica de Catalunya, Eduard Maristany, 10-14, 08019 Barcelona, Spain

[§]Laboratoire de Chimie Physique des Biomolécules, Unité de Chimie Physique Théorique et Structurale (UCPTS), University of Namur, Rue de Bruxelles, 61, 5000 Namur, Belgium

Supporting Information

ABSTRACT: The thermomechanical response of Omp2a, a representative porin used for the fabrication of smart biomimetic nanomembranes, has been characterized using microcantilever technology and compared with standard proteins. For this purpose, thermally induced transitions involving the conversion of stable trimers to bigger aggregates, local reorganizations based on the strengthening or weakening of intermolecular interactions, and protein denaturation have been detected by the microcantilever resonance frequency and deflection as a function of the temperature. Measurements have been carried out on arrays of 8-microcantilevers functionalized with proteins (Omp2a, lysozyme and bovine serum albumin). To interpret the measured nanofeatures, the response of proteins to temperature has been also examined using other characterization techniques, including real time wide angle X-ray diffraction. Results not only demonstrate the complex behavior of porins, which exhibit multiple local thermal transitions before undergoing denaturation at temperatures higher than 105 °C, but also suggest a posttreatment to control the orientation of immobilized Omp2a molecules in functionalized biomimetic nanomembranes and, thus, increase their efficacy in ion transport.

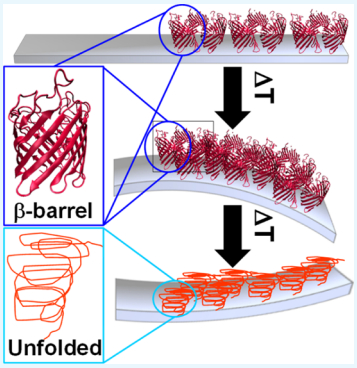

INTRODUCTION

Recently, there has been a paradigmatic shift in the experimental study of materials with applications in biomedicine: new methods have been developed to study phenomena associated to single molecules and their small supramolecular/nanostructured aggregates when embedded within complex platforms with functional interfaces for clinical applications. In particular, micro- and nanosized mechanical techniques, based on the principle that variations in electrostatic, van der Waals, and steric intermolecular interactions on the surface of functionalized cantilever cause bending (deflection) of a few nanometers, are playing a fundamental role.[1] The combination of these miniaturized mechanical systems with electrical and, especially, optical displacement sensors has been applied for, among others, chemisorption measurements in air at room temperature with up to yoctogram (10^{-24} g) resolution,[2,3] drug screening,[4,5] characterization of the thermomechanical response and the glass transition temperatures of macromolecular ultrathin films,[6,7] detection of DNA strands,[8] observation of the hydration−dehydration (swelling−deswelling) of molecular systems,[9−11] and identification of biological species through their molecular mass and stiffness, improving the capabilities of conventional mass spectrometers.[12,13]

Porins are β-barrel outer membrane proteins (OMPs) that form water-filled open channels and allow the passive penetration of hydrophilic molecules. Because of their capacity in exchange ions and small nutrients (i.e., typically <667 Da) over the outer membrane, porins have been used to fabricate smart biomimetic nanomembranes (NMs) that could incorporate biological functions, such as controlled ion transport.[14] For this purpose, OMPs are immobilized onto supported organic or inorganic NMs,[15−18] or even confined inside synthetic pores.[19−21] Apparently, in all cases, the nanostructured porin aggregates formed in the resulting biointerfaces play a crucial role in the selective ion permeability. However, the size and shape of these structures are drastically influenced by the chemical environment, being usually different from those found in the natural state. For example, the individual trimeric units found in natural environments for Omp2a,[22,23] a β-barrel OMP from *Brucella melitensis*, self-

Received: March 12, 2018
Accepted: July 2, 2018
Published: July 13, 2018

DOI: 10.1021/acsomega.8b00463
ACS Omega 2018, 3, 7856−7867

associate into hierarchical structures with around 6−8 trimeric units when the protein incorporates onto the surface of supported NMs or inside the synthetic pores of polymeric free-standing NMs for biosensing, nanofluidics, and ion-rectifying for energy conversion.[17,21]

In this study, we investigated the organization of β-barrel OMPs in synthetic environments as a function of the temperature, thereby applying microcantilever deflection technologies to hierarchical structured Omp2a (367 residues, 39 kDa). The interpretation of these measurements has been carried out with the aid of the results obtained using other techniques, such as Fourier transform infrared (FTIR) spectroscopy, circular dichroism (CD), dynamic light scattering (DLS), wide angle X-ray diffraction (WAXD), X-ray photoelectron spectroscopy (XPS), and atomic force microscopy (AFM). The distinctive thermal transitions identified for Omp2a, which compare with those observed for conventional proteins such as lysozyme (LYS; 129 residues, 14.4 kDa) and bovine serum albumin (BSA; 583 residues, 66.5 kDa), have been unraveled and their consequences and effects analyzed.

METHODS

Materials. Octosensis microcantilever arrays (chips with eight monocrystalline Si cantilevers, 500 μm in length) were obtained from Micromotive GmbH (Mainz, Germany). The following chemicals were purchased from Sigma-Aldrich and used as received without further purification: isopropanol, (3-glycidyloxypropyl)trimethoxysilane (98%); toluene (99.8%); N^{α},N^{α}-bis(carboxymethyl)-L-lysine hydrate (NTA−NH_2) (97%); 1-[(3-dimethylamino)propyl]-3-ethylcarbodiimide methiodide (EDC); *N*-hydroxysuccinimide (NHS), 2-(*N*-morpholino)ethanesulfonic acid (MES); 2-amino-2-(hydroxymethyl)-1,3-propanediol (Tris base); carbonate/bicarbonate buffer; and phosphate buffered saline (PBS, pH 7.4). Sodium chloride was purchased from Panreac (Spain). BSA (fraction V) and LYS were purchased from BioLabs (England) and Fluka, respectively. The Omp2a protein was expressed, purified, and refolded using a previously reported procedure.[22,23]

FTIR Spectroscopy. FTIR spectra of BSA, LYS, and Omp2a were recorded on a FTIR 4100 Jasco spectrophotometer. The samples were placed in an attenuated total reflection accessory with thermal control and a diamond crystal (Specac model MKII Golden Gate Heated Single Reflection Diamond ATR). For each sample, 46 scans were performed with a resolution of 4 cm^{-1}. Spectra were recorded at 30 and 100 °C.

FTIR spectroscopy was used to examine the secondary structure of the proteins. Specifically, the number and position of the peaks in the amide I region, which were derived from the second derivative and deconvoluted spectra, provided information about the protein conformation. Fourier self-deconvolution was performed with the software PeakFit 4 (Jandel Scientific Software, AISN Software Inc.), the resulting profiles being fitted to Gaussian functions through the OriginPro 7.5 software.

Circular Dichroism. CD measurements of BSA and LYS were performed using 1× commercial Dulbecco's PBS from Gibco with a protein concentration of 0.01 mg/mL, whereas a sodium dodecyl sulfate (SDS)−2-methyl-2,4-pentanediol (MPD) buffer (60 mM SDS, 1.5 M MPD, 400 mM NaCl, 50 mM Tris-HCl pH 8) with a protein concentration of 0.005 mg/mL was used for Omp2a. It should be noted that the different buffer selection is due to the fact that the Omp2a structure is protected by amphiphilic SDS−MPD detergents.[22,23] Spectra were recorded between 190 and 250 nm using a Chirascan-plus *q*CD spectrometer (Applied Photophysics, APL; UK) equipped with a temperature-controlled cell. Spectra were obtained using heating (from 5 to 90 °C) and cooling (from 90 to 5 °C) runs stopping every 5 °C for 5 min with a heating rate of 5 °C/min. Machine settings were as follows: 1 nm bandwidth, 1 s response, 0.5 nm data pitch, 100 nm/min scan speed, and cell length of 10 mm. All CD spectra presented in this work correspond to the average from three different runs. Spectra were deconvoluted using the CDSSTR method of the DichroWeb server.[24]

Dynamic Light Scattering. The influence of the temperature on the shape and aggregation of BSA, LYS, and Omp2a was studied by DLS, following the variation of the particle effective diameter (D_{eff}) when the temperature increases from 20 to 60 °C. Proteins were dissolved in the buffers described above for CD measurement using the same concentrations. Measurements were performed using a NanoBrook Omni Zeta Potential Analyzer from Brookheaven Instruments Corporation. D_{eff} values correspond to average values of the corresponding particle size distributions, which were determined in steps of 10 °C (heating/cooling rate 10 °C/min) stopping for 2 min before the measurement.

Wide-Angle X-ray Diffraction. Time-resolved WAXD experiments were carried out at the NCD beamline (BL-11) of the Alba synchrotron radiation light facility of Cerdanyola del Vallès (Catalunya). The beam was monochromatized to a wavelength of 1.5406 Å. Samples were confined between Kapton films and then held in a Linkam hot stage with temperature control within ±0.1 °C. WAXD profiles were acquired during heating and cooling runs in time-frames of 7.5 s and a rate of 4 °C/min. The WAXD detector was calibrated with diffractions of a standard of a Cr_2O_3 sample. The diffraction profiles were normalized to the beam intensity and corrected considering the empty sample background. Deconvolution of WAXD peaks was performed with the PeakFit v4 program by Jandel Scientific Software using a mathematical function known as "Gaussian area".

Functionalization of Silicon Microcantilever Chips. The functionalization protocol, which was applied to silicon microcantilever chips previously hydroxylated at the surface with a H_2O_2/H_2SO_4 (3:1 v/v) mixture, consisted of four steps

(i) Silanization: Hydroxylated microcantilevers were silanized with 0.2% of (3-glycidyloxypropyl)trimethoxysilane in dry toluene overnight at room temperature under a nitrogen atmosphere. Afterward, samples were washed with toluene and Milli-Q water.

(ii) Carboxylation: Silanized microcantilevers were incubated into 100 mM N^{α},N^{α}-bis(carboxymethyl)-L-lysine hydrate (NTA−NH_2) solution in 50 mM carbonate buffer (pH 9.5) overnight, at room temperature, and under gentle agitation. After this, carboxylated substrates were washed with 50 mM carbonate buffer (pH 9.5) and Milli-Q water.

(iii) Activation: The carboxyl groups arising from NTA−NH_2 at the microcantilever surface were activated for direct reaction with primary amines via amide bond formation with a mixture of 100 mM EDC and 150 mM NHS, both dissolved in 10 mM MES (pH 5.5). Samples were incubated for 30 min at 37 °C under gentle

DOI: 10.1021/acsomega.8b00463
ACS Omega 2018, 3, 7856−7867

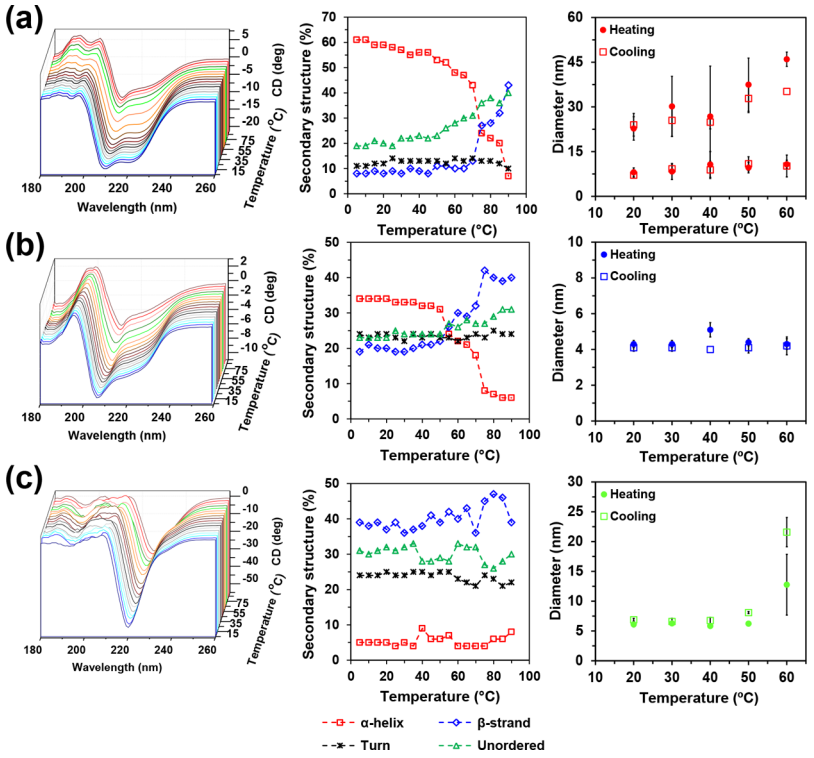

Figure 1. CD spectra (left) recorded for (a) BSA, (b) LYS, and (c) Omp2a proteins at temperatures ranging from 5 to 90 °C (heating runs). Measurements for BSA and LYS were performed using a carbonate buffer, whereas a SDS−MPD buffer was used for Omp2a (Supporting Information). The variation of amount of secondary structures (in %) against the temperature is also represented (middle). Effective diameter (right) derived from DLS measurements at temperatures ranging from 20 to 60 °C (measures for heating and cooling runs are displayed) for (a) BSA, (b) LYS, and (c) Omp2a proteins. Two profiles are displayed for BSA because a bimodal distribution was found for all examined temperatures, while a unimodal histogram was observed for both LYS and Omp2a.

agitation and, then, extensively rinsed with 10 mM MES (pH 5.5).

(iv) Protein immobilization: A solution of 0.1 mg/mL of protein (BSA, LYS or Omp2a) was prepared in 10 mM MES (pH 5.5). The cantilevers were incubated for 2 h at 37 °C. After that, the samples were washed with 10 mM MES (pH 5.5) and incubated for 45 min at 37 °C with 1× PBS with 0.3 M NaCl to desorb proteins not covalently bonded to the surface.

X-ray Photoelectron Spectroscopy. XPS was used to analyze the chemical composition at the surface of silicon substrates. The system (SPECS Surface Nano Analysis GmbH, Berlin, Germany) was equipped with a nonmonochromatic twin anode X-ray source XR50 of Mg/Al (1253 eV/1487 eV). Specifically, the Al anode was operated at 150 W. Detector pass energy was set at 25 and 0.1 eV for the survey and the narrow scans (high resolution spectra), respectively, at a pressure below 7.5×10^{-9} mbar. Casa XPS software (Version 2.3.16, Casa Software Ltd., Teignmouth, UK) was used to fit and perform peak integration of spectra. The C 1s peak was used as an internal reference (284.8 eV). High resolution XPS spectra were acquired by Gaussian−Lorentzian curve fitting after S-shape background subtraction.

Wettability. Contact angle measurements were conducted using the water drop method. Milli-Q water drops (0.5 μL) were deposited onto the surface of the substrate and recorded after stabilization with the equipment OCA 15EC (Data-Physics Instruments GmbH, Filderstadt). The SCA20 software was used to measure the contact angle, which is shown in this work as the average of at least 10 measures for each sample.

Atomic Force Microscopy. AFM was conducted to obtain topographic images of the nonfunctionalized and functionalized surfaces using Si TAP 150-G probes (Budget Sensors, Bulgaria) with a frequency of 150 kHz and a force constant of 5 N/m. Images were obtained with an AFM Veeco Multimode under ambient conditions in tapping mode. The row scanning frequency was set between 0.6 and 0.8 Hz. The root-mean-square roughness was determined using the statistical application of the NanoScope Analysis software (1.20, Veeco).

Resonance Frequency Measurements and Cantilever Displacement. Cantilever resonance frequency and displacement measurements were carried out by means of the SCALA equipment (Scanning Laser Analyzer, from MecWins), a recently developed technology for the optical readout of cantilevers.[7,25,26] The readout technique combines the optical beam deflection method and the automated two-dimensional scanning of a single layer beam by voice-coil actuators. The equipment has been implemented with a thermal chamber containing a thermoelectric cooler and a cartridge heater. These elements are capable of sweeping the chamber's temperature from −50 °C up to 220 °C by flowing thermostatized N_2 to the sample. A holder containing multiple thermometer probes is placed inside the chamber for a better mapping of the temperature. All measurements were performed in a nitrogen environment. The temperature control was regulated by software created by the MecWins Company.

Monocrystalline Si microcantilever chips containing arrays of eight cantilevers (Micromotive GmbH) were used for the nanomechanical measurements (Supporting Figure 4A). Specifically, the nominal length, width, and thickness of the

DOI: 10.1021/acsomega.8b00463
ACS Omega 2018, 3, 7856−7867

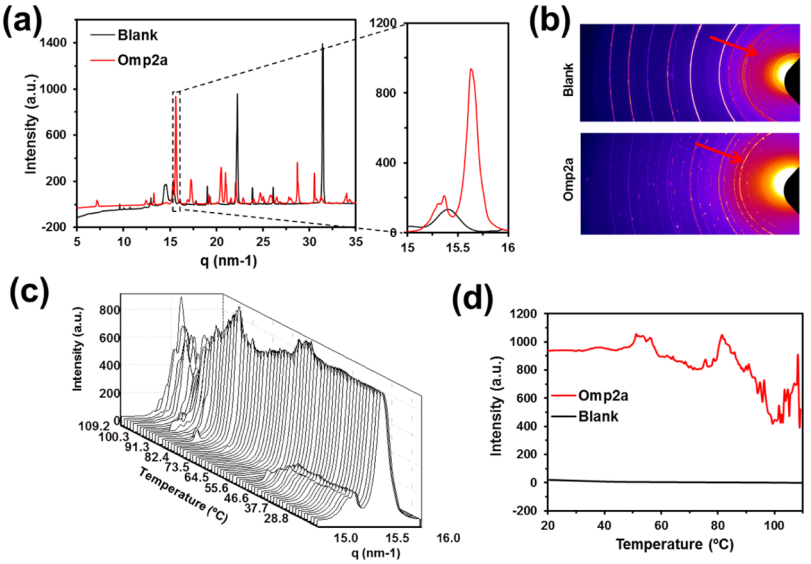

Figure 2. (a) 1D scattering patterns of blank (salts from the buffer solution) and Omp2a samples as dry powder at room temperature. (b) 2D scattering patterns of the blank and Omp2a dried samples at room temperature. (c) 1D scattering pattern of Omp2a when a temperature ramp (heating) is applied. (d) Intensity of the peak profile for the blank and the Omp2a samples at q = 15.6 nm^{-1} during the temperature ramp.

cantilevers were 500, 90 ± 2, and 1 μm, respectively. Resonance frequency measurements were conducted in a nitrogen atmosphere at 25 °C. The experimental setup is based on the shift induced in the resonance frequency by the added mass onto the cantilever through functionalization. The used platform consists in the automated two-dimensional scanning with a single laser (1 mW) beam by voice-coil actuators perpendicularly located. Displacements over a range of several millimeters at speeds up to 10 mm/s and with an accuracy of 100 nm are achieved. Once the laser beam is reflected by the cantilever array, the exact position and intensity of the reflected spot are collected by a two-dimensional linear position detector. Moreover, TRACKER, which is an algorithm that recognizes reflected intensity patterns, locates cantilever sensors in a fully automated process.

RESULTS

The response of Omp2a to thermal stress has been compared with those of BSA and LYS. The latter exhibits an ellipsoidal shape in which both ordered (30% α-helix, 27% β-turn and 13% β-sheet secondary structures) and unordered (30%) regions coexist,[27] while the BSA structure is predominantly α-helical with the remaining polypeptide occurring in turns and extended or flexible regions (i.e., with no β-sheets).[28] Before nanomechanical measurements, the effects of the heat shift on the secondary structure and aggregation tendency of such three proteins have been examined.

Secondary Structure and Diameter. Temperature-induced protein denaturation is frequently detected using FTIR spectroscopy and CD in various wavelength regimes. The vibrational spectrum is selective in the absorption band frequency position, widths, and intensities in response to protein structural changes.[29] Specifically, the amide I band (1700−1600 cm^{-1}), which convolutes the major structural domain elements of proteins, including α-helix, β-sheet, β-turn, and random coil (unstructured), has been used to visualize the response of BSA, LYS, and Omp2a to heating (Figure S1 displays the FTIR spectra recorded at 30 and 100 °C). At high temperatures, both BSA and LYS underwent a drastic unfolding, as is reflected by the apparition of an intense deconvoluted peak at ∼1640 cm^{-1} that has been associated to the unstructured protein. In contrast, the resemblance between all spectra recorded for Omp2a suggests that the β-barrel structure is preserved at the highest temperature.

FTIR observations are fully consistent with the CD spectra (Figure 1) recorded in heating runs from 5 to 90 °C, which reflect an increment of the disordered motifs at temperatures higher than ∼55 °C for both BSA and LYS while the content of ordered secondary structures, especially α-helix, decreases. The unfolding temperature estimated from CD results is 67 and 65 °C for BSA and LYS, respectively. These results are fully consistent with those reported earlier by different authors for LYS in aqueous solution.[30,31] Specifically, it was concluded that the protein loses a small part of helical structures in the α-domain below 64 °C, undergoing irreversible (unless cooling start just after reaching ∼80 °C) thermal unfolding of the secondary structures at a temperature close to 75 °C. Instead, Omp2a only exhibits slight variations (i.e., thermal stress) in the secondary structures, the amount of unstructured protein remaining practically constant from 5 to 90 °C. Moreover, the thermal behavior of the three proteins is reversible, as is evidenced from the analyses of the CD spectra recorded in cooling runs (Figure S2).

The influence of the temperature on the shape and aggregation of the proteins was assessed by DLS. Profiles displaying the variation of the particle effective diameter (D_{eff}) with the temperature are included in Figure 1 (both heating and cooling runs). Bimodal distributions were found for BSA at all examined temperatures, and therefore, two D_{eff} profiles are displayed in Figure 1a. In the first one, which corresponds to individual BSA molecules, D_{eff} grows from 8.1 ± 1.4 nm at 20 °C to 10.7 ± 1.4 nm at 60 °C, evidencing that the unfolding process is accompanied by an increment of the molecular dimension. The D_{eff} values of the second profile are approximately 3 times the values of the first one, indicating that BSA also forms trimers. In this case, D_{eff} increases from 23 ± 4 nm at 20 °C to 46 ± 2 nm at 60 °C. In contrast, LYS presents unimodal distributions, independently of the temper-

DOI: 10.1021/acsomega.8b00463
ACS Omega 2018, 3, 7856−7867

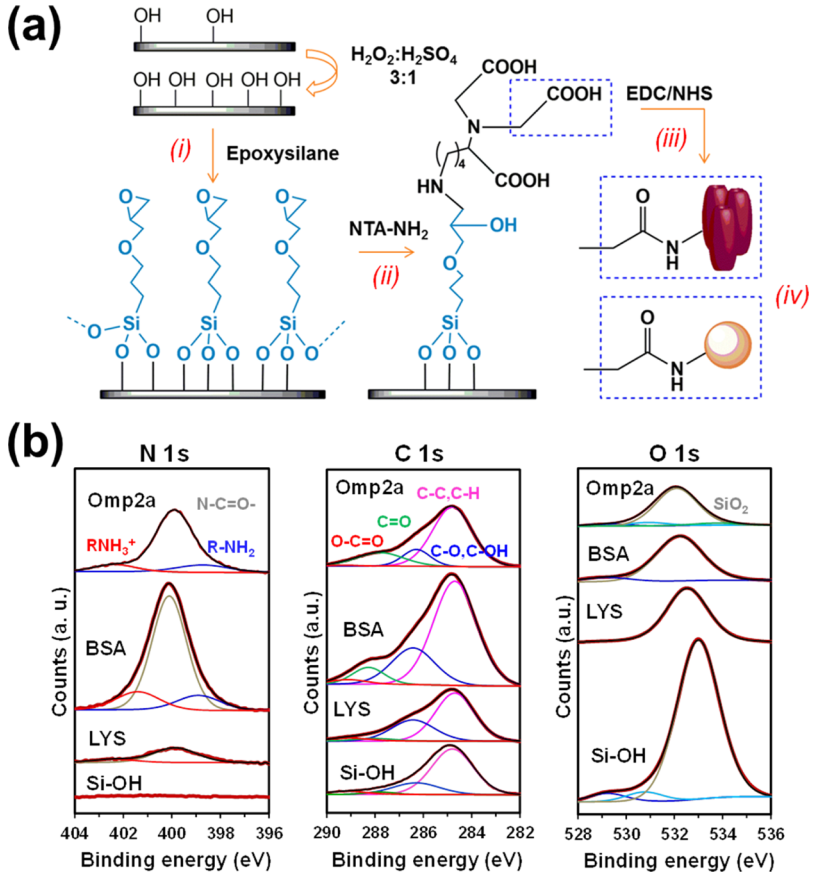

Figure 3. (a) Protein functionalization protocol for silicon substrates. (b) N 1s, C 1s, and O 1s high-resolution XPS spectra for nonfunctionalized (hydroxylated; Si−OH) and protein-functionalized (LYS, BSA, or Omp2a) silicon substrates. Peaks from deconvolution are also displayed.

ature, with similar D_{eff} values (i.e., 4.3 ± 0.2 nm and 4.3 ± 0.5 nm at 20 and 60 °C, respectively). Although these results suggest that LYS volume is not affected by the unfolding, what actually occurs is that unfolding is accompanied by a reduction in the hydration. The latter was proved in early X-ray scattering studies at 20 and 80 °C,[30] which showed that the electron density of water in LYS crystals decreases with the crystallization temperature, and consequently, the radius of gyration remained practically invariant. Thus, we hypothesize that changes in protein hydration offset the thermally induced protein motion. Similar observations have been found for other proteins,[32] negative volume changes being detected in some cases.[33]

Finally, Omp2a also presents a unimodal distribution, even though D_{eff} increases when the 6.1 ± 0.2 nm at 20 °C to 12.6 ± 2.4 nm at 60 °C. The former value has been associated to the trimeric state, while the latter corresponds to bigger aggregates.[21] The thermal stability observed for Omp2a combined with this significant variation, which is even higher in the cooling run (i.e., from 21.6 ± 5.1 nm at 60 °C to 6.9 ± 0.4 nm at 20 °C), indicates that the reversible aggregation of this OMP is notably enhanced by the temperature. Thermomechanical assays combined with these DLS results have been used to explain the aggregation phenomena of Omp2a in the Discussion section.

Time-Resolved WAXD Data on Heating and Cooling of Lyophilized Omp2a. Real-time WAXD experiments were performed using synchrotron radiation to examine the evolution of the β-sheets motifs in dried Omp2a during heating and cooling processes. Analyses were performed considering both Omp2a and blank samples, which were obtained by freeze-drying the detergent buffer solution in the presence and absence of protein, respectively. The one-dimensional WAXD profile acquired for Omp2a at room temperature exhibits a sharp and intense peak at q = 15.64 nm^{-1} (Figure 2a), which corresponds to an interstrand spacing of d = 4.02 Å.[34,35] This peak is absent in the spectra recorded for blank samples, the broad peak centered at q = 15.40 nm^{-1} being attributed to the salts from the buffer (Figure 2a, magnification). The presence and absence of the reflection associated to the β-sheet in the Omp2a and blank samples, respectively, is clarified in the representative diffraction patterns showed in Figure 2b.

Figure 2c displays a three-dimensional representation of the freeze dried Omp2a WAXD profiles in the β-sheet region (q = 15−16 nm^{-1}) obtained by heating at a rate of 5 °C/min from 25 to 110 °C, whereas Figure 2d represents the variation in intensity of the peak at q = 15.6 nm^{-1} that occurs when heating both for Omp2a and blank samples. The variation with temperature of this narrow and intense peak has been used to monitor the effect of the different thermally induced structural processes in interstrand interactions. First, the intensity experiences a small increment at 50−55 °C, which has been attributed to the reinforcement of neighboring intermolecular connections. According to DLS observations, which evidenced the transition from the trimeric form to bigger aggregates (Figure 1c), this result has been interpreted as the formation of new β-sheets between neighboring protein molecules. After this, from ∼55 to ∼75 °C the intensity decreases slowly and, suddenly, grows again at ∼80 °C. These changes suggest the

DOI: 10.1021/acsomega.8b00463
ACS Omega 2018, 3, 7856−7867

restructuration of the newly formed aggregates during the heating process. Finally, the peak progressively broadened and becomes less intense at higher temperatures, evidencing that temperature has some effects in the local stability of the β-sheets. In spite of this, the peak maintains 47% of its initial intensity at 100 °C, which is consistent with the overall stability of the β-barrel structure observed above by FTIR (Figure S1c).

Protein Immobilization onto the Surface of Silicon Microcantilevers. The microcantilever-based biosensing technology has been applied in this work to monitor the response of OMPs in synthetic environments against the temperature change. Analysis of the results has been carried out by comparing their thermal behavior with conventional proteins. Among other features, this nanomechanical platform is characterized by the high sensitivity, label-free detection, and small sample consumption because of the size of the microcantilevers (ca. 1000 μm^2).[36] For successful characterization, the first step is the functionalization of silicon microcantilevers to achieve a stable and irreversible protein−surface binding.

In this work, a recently developed procedure to covalently bind small peptides to silicon has been extrapolated and adapted to BSA, LYS, and Omp2a proteins (Figure 3a).[37] This four-step protocol can be summarized as follows: (i) the microcantilever surface, previously hydroxylated with acids, is silanized with (3-glycodyloxypropyl)trimethoxysilane; (ii) epoxy groups are opened with N^{α},N^{α}-bis(carboxymethyl)-L-lysine hydrate (NTA−NH_2) at basic pH; (iii) the carboxylated surface derived from (ii) is activated with a mixture of EDC and NHS; and (iv) proteins are immobilized by incubating the activated surface in the corresponding protein solution. Before conducting any measurement, proteins not covalently bonded to the substrate were desorbed by washing with a phosphate buffer solution. Because the three proteins investigated contain a relatively large number of amine groups, corresponding to multiple lysine residues, in addition to the *N*-terminal amine, the study of protein-overhang interactions is limited by this immobilization procedure.

Comparison of the characteristic XPS spectra in the N 1s, C 1s, and O 1s regions of hydroxylated (nonfunctionalized) silicon and protein-functionalized substrates (Figure 3b) chemically proves the success of the immobilization protocol. The presence of a peak in the C 1s region of the nonfunctionalized silicon spectrum has been attributed to the presence of organic contaminants from the environment. While the latter makes more difficult the corroboration of the protein incorporation, the carbon content is significantly higher when silicon was functionalized with BSA, LYS, and Omp2 (Table S1), showing a 4.5, 3.0, and 3.2 fold increase, respectively. Moreover, the apparition of the N 1s peak, which was not detected for nonfunctionalized substrates, is an unequivocal chemical evidence of the protein immobilization (Table S1). Changes in surface properties, as for example the wettability (Figure 4a) and the surface topography (Figure 4b), provide indirect evidence of the binding between the substrate and the protein. Thus, contact angle (θ) measurements using milli-Q water showed that the hydrophilic character of silicon (θ = 30° ± 5°) decreased considerably upon the incorporation of protein (θ = 70° ± 3°, 47° ± 2°, and 49° ± 6° for BSA, LYS, and Omp2a, respectively). Similarly, 3D topographic AFM images reveal significant differences between the bare silicon substrate and the functionalized ones,

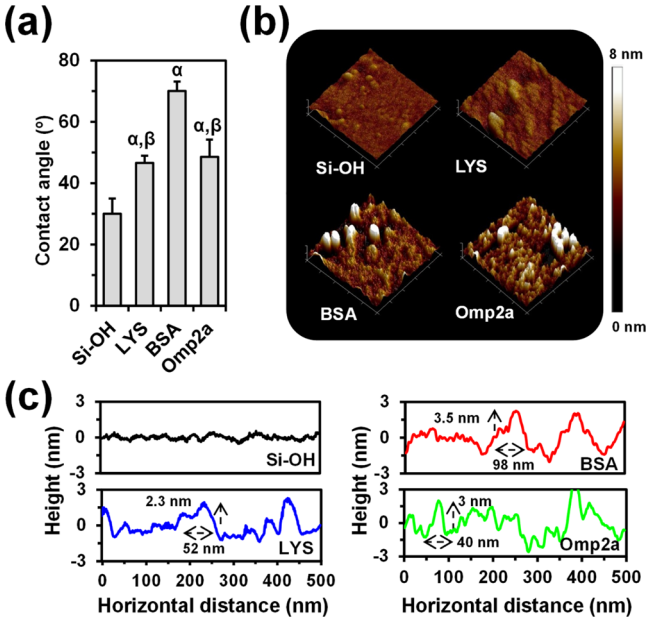

Figure 4. (a) Average contact angle of nonfunctionalized and functionalized silicon substrates. Greek letters on the columns refer to significant differences when 1-way ANOVA and Tukey's multiple comparison tests are applied: α vs Si−OH ($p < 0.0001$) and β vs BSA ($p < 0.0001$). (b) Topographic AFM images of nonfunctionalized and functionalized substrates (500 × 500 nm^2). (c) Representative cross-sectional profiles for AFM images.

which affect the root-mean-square roughness (Figure S3). Moreover, inspection of the cross-sectional profiles (Figure 4c) is consistent with the immobilization not only of individual protein molecules but also of aggregates, diameter sizes ranging from 40 to 98 nm.

Thermomechanical Response of Protein-Functionalized Microcantilevers. Protein-functionalized silicon chips with arrays of eight cantilevers (i.e., using such number of sensors in parallel) were operated in dynamic mode (Figure S4a). Piezoelectric excitation (i.e., an actuator is positioned below the chip base) and their first vibration mode were monitored by using a scanning laser. After cleaning with isopropanol and hydroxylation with a H_2O_2/H_2SO_4 (3:1 v/v) mixture, hydroxylated chips (100 μm wide, 500 μm long and 1 μm thick) displayed a resonance frequency of 5206 ± 162 Hz (n = 16) measured in a N_2 atmosphere at 25 °C.

Figure 5a shows the resonance frequency shift of at least 16 LYS-, BSA-, and Omp2a-functionalized cantilevers. As it can be seen, the frequency shift value is significantly higher for Omp2a than for BSA and LYS. Provided the molecular weight of Omp2a is smaller than that of BSA (i.e., 39 kDa vs 66.5 kDa), the formation of relatively big supramolecular aggregates is clearly evidenced. This feature is corroborated by comparing nanomechanical first mode resonances of hydroxylated and functionalized cantilevers (Figure S5), which provides a shift of 92, 182, and 313 Hz for LYS, BSA, and Omp2a, respectively. On the other hand, the standard error of the mean calculated for Omp2a is significantly higher than for LYS and BSA. This has been attributed to the variability in the size of the Omp2a supramolecular aggregates, which induces fluctuations in the measured frequency shift values. However, it should be remarked that differences among LYS, BSA, and Omp2a are large enough to be independent of such uncertainty.

DOI: 10.1021/acsomega.8b00463
ACS Omega 2018, 3, 7856−7867

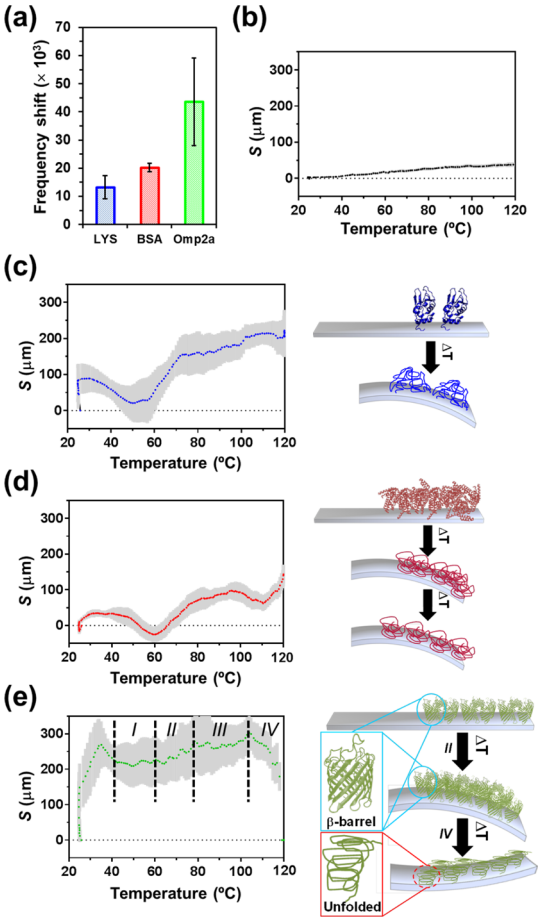

Figure 5. (a) Nanomechanical response, expressed as resonance frequency shift ($|\Delta f|/f$), of functionalized cantilevers (mean values and standard error of the mean calculated with the data of at least 16 different cantilevers). (b) Relative displacement as a function of the temperature of a representative hydroxylated (nonfunctionalized) cantilever. Thermomechanical response of cantilevers functionalized with (c) LYS, (d) BSA, and (e) Omp2a proteins. Right: mean relative displacement as a function of the temperature (blue, red, and green dots in c, d, and e, respectively) and the corresponding standard error of the mean (thick light-gray lines), both calculated with the data of at least seven different cantilevers, are displayed at the right. Left: cartoons schematizing the folded → unfolded transitions in c and d, and the trimer → large aggregate and β-barrel → unfolded transitions in e. The four regions described in the text are labeled in e.

The thermal response of proteins have been analyzed by plotting the displacement (S) of the reflected laser spot on the position sensitive detector (PSD), which originates from the variation of the local slope at the cantilever surface with the temperature and depends on the distance (D) between the cantilever and the PSD (Figure S4b). It is worth noting that the variation of S with the temperature is analogous to the thermally induced cantilever deflection (Δz). As it was expected, the displacement of nonfunctionalized cantilevers increases slowly and progressively with the temperature (Figure 5b), as the deflection of rectangular bare cantilevers of length L grows linearly with the change of temperature (ΔT), that is, $\Delta z \propto L^2 \Delta T$.[38]

The average displacement curve obtained for LYS (Figure 5c), which was obtained using 16 different microcantilever sensors, reflects a behavior very different from that obtained for nonfunctionalized cantilevers. The slope of the displacement curve in the region comprised from room temperature to ∼50 °C is related to the deflection produced by the different thermal response of the two materials contained in the system (i.e. the silicon substrate and the attached protein). More specifically, protein-functionalized cantilevers undergo a differential stress due to the thermal expansion coefficient difference between the protein and the microcantilever itself, giving rise to the cantilever deflection. After this, at ∼50 °C the protein starts to unfold, causing a redistribution of the molecular mass and altering the contact between the protein and the substrate. This situation enhances the cantilever deflection, as it is reflected by the sustained increasing displacement of the profile displayed in Figure 5c. Thus, the melting temperature of LYS, as determined thermomechanically, is approximately 60 °C, which is consistent with the CD data (Figure 1). At ∼70 °C the slope of the displacement curve changes and the curve is similar to that observed for the hydroxylated silicon cantilevers (Figure 5b). Thus, once LYS completes the conversion toward the unfolding state, the changes induced by the thermal dynamics of the random coil are not reflected in the deflection. At this stage the effects associated to the mass redistribution and the variation of the protein···surface interactions are negligible in average. Overall, the profile displayed in Figure 5c should be considered as the fingerprint to recognize the thermomechanical response of conventional proteins, in which the folded → unfolded is the only occurring thermal transition.

Figure 5d displays the average displacement curve achieved for BSA. From a qualitative point of view, the behavior of the curve is similar to that described above for LYS until ∼100 °C, even though the cantilever deflection is smaller for BSA. This has been attributed to the higher molecular weight of BSA and its tendency to aggregate, both reducing the differences in the stress distribution and the stress gradient between the protein and the substrate. Consequently, the impact of the bimetallic effects in the bending of the cantilever is relatively small before the protein denaturation at ∼60 °C. Moreover, the effect of the redistribution of the molecular mass during the unfolding process is also smaller than for LYS. As the effect of the unfolding on the cantilever displacement is expected to be directly proportional to the amount of protein molecules, these results suggest that such amount is lower for cantilevers functionalized with BSA than with LYS. Although this could be in apparent contradiction with the nanomechanical first mode resonance shift, which is 90 Hz lower for the latter (Figure S5), it is worth noting that the molecular weight of BSA is 4 times higher than that of LYS.

In spite of this, the dynamics of the random coil causes a change in the sense of the cantilever deflection. Thus, deflection downward or upward of the cantilever is mainly defined by the response of the protein within the studied temperature range, and as mentioned above, the deflection was relatively low before the unfolding. After this, the upward profile experiences an abrupt change at ∼110 °C, which is not detected for LYS. Although this sudden drop in the displacement could be hypothesized as a disaggregation of the protein molecules, a simple thermogravimetric analysis (not shown) evidenced that it corresponds to the evaporation of water molecules that were strongly interacting with the protein. Accordingly, in addition to the molecular unfolding, thermomechanical characterization of BSA reveals a sharp dehydration process that, suddenly, produces a change of sign in the stress gradient.

DOI: 10.1021/acsomega.8b00463
ACS Omega 2018, 3, 7856−7867

The displacement profile recorded for Omp2a (Figure 5e) exhibits unusual complexity. Although bimetallic effect initially affects the cantilever deflection, as in LYS and BSA, four regions with distinctive regimes can be distinguished above 40 °C for Omp2a. In the first one, which extends from 40 to 60 °C, the variation of the displacement is practically null, suggesting that the redistribution of the molecular masses and the changes in the protein···substrate interactions are minimum (region I in Figure 5e). From a microscopic point of view, this region has been associated with the alteration of intermolecular interactions before the transition from trimers to bigger aggregates, which is also consistent with WAXD observations (Figure 2d). While initially they seem to become more intense, the step prior to the conversion into bigger aggregate is characterized by a weakening of interactions among neighboring Omp2a molecules in trimers. This phase transition is evidenced by the increasing displacement (region II in Figure 5e), which occurs in a relatively wide interval of temperatures (i.e., between ∼60 and ∼77 °C). After this (region III in Figure 5e), the displacement experiences small fluctuations, the average deflection increment along the whole region being very small. These fluctuations have been associated with local re-organizations in the newly formed aggregates. Above 105 °C, the displacement drops sharply (region IV in Figure 5e), suggesting that at such high temperatures the thermal stability of the β-barrel is finally lost. Therefore, the downward deflection of the cantilevers is a consequence of the folded → unfolded transition that alters both the mass distribution and the Omp2a···substrate interactions. These observations are fully consistent with the WAXD results displayed in Figure 2d.

DISCUSSION

Although the secondary structure of bacterial OMPs are known to be very sensitive to the polarity of the environment, they exhibit an increased thermal stability that has been typically attributed not only to the abundant β-strands barrel but also to their oligomeric architectures.[39−42] However, complete understanding of the thermal response of their supramolecular oligomeric architectures in synthetic environments, which is essential for the utilization of OMPs in the fabrication of bioinspired nanodevices, is an unresolved question.[43]

Our FTIR and CD results on Omp2a prove that the efficient interstrand hydrogen bond network preserves the protein secondary structure from thermal unfolding even outside lipid environments similar to those found in nature. Besides, the heat-induced CD response of secondary structural elements in Omp2a has also been compared with that of conventional proteins. In folded proteins, the α-helix is recognized by minima at ∼220 and ∼210 nm, while the β-sheet has a minimum at 218 nm and a maximum at ∼195 nm.[44] These two structural motifs are detected in the spectra recorded for LYS and Omp2a at room temperature, whereas the spectrum of BSA mainly involves the helical motif. However, the structural signatures of BSA and LYS significantly change beyond ∼55 °C, evidencing the loss of secondary structure,[45] while the CD spectrum of Omp2a remains practically unaltered until 90 °C.

On the other hand, DLS data reflect that Omp2a self-associates into the typical trimeric state found in the outer membranes of bacteria in the detergent buffer at room temperature. Thus, the D_{eff} measured by transmission electron microscopy (TEM) for Omp2a trimers in dried samples was recently found to be 9.3 ± 3.0 nm,[21] which is consistent with DLS value at 20 °C (6.1 ± 0.2 nm). However, the formation of bigger aggregates is detected by DLS when the temperature increases above 50 °C, even though they are significantly smaller (D_{eff} = 12.6 ± 2.4 nm) than those also observed in dried samples at room temperature (D_{eff} = 25.9 ± 4.8 nm) by TEM.[21] Thus, the van der Waals interactions between the side groups at the external side of the β-barrel are promoted through both drying and heating. This feature points out the importance of improving the understanding of Omp2a self-association processes in non-native environments, as for example those used to fabricate bioinspired NMs for ion transport.

WAXD experiments indicate that temperature affects the β-sheet structure of Omp2a. This effect is focused in intermolecular interactions at temperatures lower than ∼80 °C and in both inter- and intramolecular interactions at higher temperatures. However, the amount of β-sheets preserved at 110 °C is still high enough to preserve the β-barrel structure, which supports FTIR and CD results. Thus, WAXD results corroborate the conversion of trimers into bigger aggregates at 50−55 °C, which after equilibration through local reorganizations remain relatively stable until ∼80 °C. At higher temperatures, intermolecular and, probably, intramolecular β-strands are affected by the thermal stress, these interactions being roughly halved. This interpretation is consistent with the well-known increased thermal stability of bacterial porins, which exhibit temperature induced unfolding above 100 °C.[39,46] This unusual stability is consequence of their β-barrel structural architecture composed of antiparallel β-sheets, in which strands are connected by long loops. Thus, the energy required to breakdown the secondary and quaternary structure of bacterial porins is significantly higher than that necessary to unfold BSA and LYS. Also, yet porin aggregates are stable, a variety of transitions associated to changes in their size (i.e., to dimers, trimers, or bigger aggregates) has been detected at temperatures significantly lower than their unfolding temperatures but comparable to the typical unfolding temperatures of conventional proteins,[46−48] which is in agreement with the opposite behaviors of Omp2a and BSA.

The D_{eff} of LYS, which remains at 4.3 ± 0.2 nm for both 20 and 60 °C, corresponds to the monomer diameter.[49,50] Thus, the mass contribution of aggregates, which are extremely difficult to avoid completely even with dilute samples, was null in the case of LYS. These features combined with CD and FTIR data indicate that the unfolding is the only thermally induced transition for LYS. Finally, BSA displays an intermediate situation with two D_{eff} values originated by the bimodal distribution observed at each temperature. The lowest value, 8.1 ± 1.4 nm at 20 °C, which is consistent with the dimensions of the prolate ellipsoid shape proposed for the protein monomer (14 × 4 nm),[49] increases by 30% with the temperature, because of the unfolding. However, the highest value, 23 ± 4 nm at 20 °C, grows more than twice when the temperature reaches 60 °C. In this case, small aggregates (dimers or trimers) not only experience unfolding processes but also incorporate more protein molecules. Accordingly, BSA self-association is promoted by the temperature when already formed aggregates act as nuclei. Overall, FTIR, CD, and DLS results probe that LYS and BSA are suitable controls for the present microcantilever deflection studies because of their different behavior not only with respect to Omp2a but also among them.

DOI: 10.1021/acsomega.8b00463
ACS Omega 2018, 3, 7856−7867

Proteins have been covalently linked via an epoxysilane-based protocol to silicon microcantilevers that had been efficiently activated by a hydroxylation treatment with a H_2O_2/H_2SO_4 mixture. The results derived from the different chemical and physical characterization techniques performed at each functionalized substrate have confirmed directly and indirectly, respectively, the suitability of the protocol to tether biomacromolecules onto the silicon surfaces. Moreover, topographic images of protein-functionalized surfaces, once biomacromolecules noncovalently bonded to the surface were eliminated, evidence heights and widths of 2−4 and 40−100 nm, respectively, demonstrating the immobilization of aggregates. As expected, the latter aggregates are much smaller and less abundant for LYS than for BSA and Omp2a, the former showing the flatter profile (root-mean-square roughness of nonfunctionalized, LYS-, BSA-, and Omp2a-functionalized substrates is 4.9 ± 2.1, 6.1 ± 2.6, 10.5 ± 5.9, and 10.7 ± 3.0 Å, respectively).

The resonance frequency of nonfunctionalized cantilevers (ω), which depends on their spring rigidity (k) and effective mass (M), is obtained by the elasticity theory as

$$\omega = \frac{1}{2\pi}\sqrt{\frac{k}{M}} \tag{1}$$

The constant k is obtained using cantilever Young modulus (E) and dimensions, length (L), width (W), and thickness (T)[51]

$$k = \frac{EWT^3}{4L^3} \tag{2}$$

Upon protein functionalization, the resonance frequency changes from ω to ν

$$\nu = \omega + \Delta\omega = \frac{1}{2\pi}\sqrt{\frac{k}{M+m} + \Gamma(k,\eta)} \tag{3}$$

where $\Delta\omega$ is the resonance frequency contribution due to the tethering of the protein, m is the mass of the protein, and Γ is a function that depends on k and the surface stress (η) induced by protein···silicon surface interactions.[52] Particularly, the difference in frequency shift ($\Delta\omega/\omega \times 10^3$) for LYS, BSA, and Omp2a was 13.2 ± 4.1, 20.2 ± 1.4, and 43.6 ± 15.6, respectively. These resonance frequency shifts suggest that protein···surface interactions predominate over m because the shift is 2 times higher for Omp2a than for BSA, whereas the molecular weight is 1.7 times higher for the latter than for the former. Accordingly, protein···surface interactions can be considered as a nanomechanical signature sensitive not only to the existence of protein aggregation phenomena but also to the distribution of the molecules in such aggregates.

In addition to the mass redistribution onto the cantilever surface, which causes changes in the resonance frequency, and to the bimetallic effect, the main mechanical effect in microcantilevers is the surfaces stress (σ) that induces a nanoscale bending.[1] This effect, which occurs if only one of both cantilever sides are coated or, as in this work, functionalized, is quantified using the Stoney's equation[53]

$$\sigma = \frac{1}{3}\left(\frac{T}{L}\right)^2\left(\frac{E}{1-\nu}\right)\Delta z \tag{4}$$

where L is the microcantilever effective length (450 μm), T is the microcantilever thickness (1 μm), E is the Young modulus of silicon (150 GPa), ν is the Poisson ratio of silicon (0.17), and Δz is the deflection of the cantilever. The surface stress is frequently associated to intermolecular interactions between molecules anchored onto the cantilever surface, such as van der Waals forces, hydrogen bonds, electrostatic interactions, steric repulsions, and so on. Ideally, protein-functionalized cantilevers should not exhibit any static surface stress if the functionalization was identical for both sides. However, in practice, the experimental setups used during the functionalization process do not result in two identical cantilever sides. As a consequence, the surface stress is not negligible for protein-functionalized cantilevers (e.g., at 120 °C, σ = 0.46 ± 0.12, 0.31 ± 0.05, and 0.30 ± 0.15 mN/m for LYS, BSA, and Omp2a, respectively; Figure S6) and significantly higher than that measured for hydroxylated nonfunctionalized ones (e.g. at 120 °C, σ = 0.08 ± 0.012 mN/m). Moreover, the surface stress experiences a significant increment when the temperature is higher than ∼50 °C for all functionalized cantilevers (Figure S7).

Analyses of the displacement curves obtained for protein-functionalized cantilevers allowed distinguishing folded → unfolded conformational transitions from phase changes related with protein aggregates. Thus, the thermally induced increment in the deflection of protein-functionalized cantilevers is not constant, as occurs for nonfunctionalized cantilevers. Proteins are much more sensitive than silicon to the temperature, and therefore, the general evolution of the displacement observed at relatively low temperatures (<50 °C) is mainly due to the differences in both stress distribution and stress gradient between the protein and the silicon substrate (i.e., the bimetallic effect). In such conditions, the bending of protein-functionalized cantilevers depends on the molecular weight and the presence of aggregates.

After this, conventional proteins exhibit an abrupt change in the evolution of the curve, which is ascribed to their denaturalization process. This folded → unfolded transition occurs at temperatures close to ∼50 and ∼60 °C for LYS and BSA, respectively, which are lower than those observed in water (60−70 °C). Consequently, in solution, the folded structure of these soluble proteins is stabilized by intermolecular hydrogen bonds with surrounding water molecules, which are loss upon removal of the solvent. This instability induces a lower unfolding temperature.

Once the denatured protein reaches a stable random coil, the dynamics of this state should not affect the thermomechanical response of the cantilever. This is true for LYS- and BSA-functionalized substrates, which show a behavior similar to that of nonfunctionalized cantilevers when the temperature exceeds ∼55 and ∼60 °C, respectively. However, BSA-functionalized cantilevers display another transition at 110 °C that has been ascribed to the evaporation of water molecules strongly interacting with protein molecules.

The thermomechanical response of Omp2a is more complex than those of LYS and BSA because of both its intrinsic thermal stability and the tendency to form not only trimers but also larger aggregates. The thermal behavior of this porin is characterized by local re-organizations, which affect the strength of intermolecular interactions among neighboring Omp2a molecules, inducing the transition from trimers to larger aggregates. The formation of such larger aggregates is consistent not only with DLS results but also with previous TEM investigations,[21] as mentioned in the Results section. The latter phase transition is poorly defined, as reflects the

DOI: 10.1021/acsomega.8b00463
ACS Omega 2018, 3, 7856−7867

continuous increase of the displacement in the temperature interval comprised between ∼60 and ∼77 °C. This feature should be attributed to the fact that the size and shape of the aggregates formed at such temperatures are constrained by the functionalization of the cantilever, which defines the tethering position of the protein molecules and gives variability to the transition. Such heterogeneity explains the undefined character of the transition that, in spite of the monodisperse and precise chemical nature of Omp2a molecules, occurs within a wide interval of temperatures rather than at a precise temperature. On the other hand, the thermal unfolding of Omp2a is detected at ∼105 °C, this temperature representing the upper threshold in relation to the manipulation of stable protein aggregates.

CONCLUSIONS

In summary, thermomechanical measurements at the microscopic level on functionalized cantilevers have provided molecular insights that complement the information obtained from conventional characterization techniques on ensembles formed by a very large number of molecules. A serious limitation of conventional techniques is that they provide only a sample average response and are unable to give information on specific local features on or within the sample. Within this context, the unique thermomechanical response of Omp2a-functionalized cantilevers, which exhibits four well-defined regimes above 40 °C (Figure 5E), suggests practical approaches to improve the efficacy of smart biomimetic NMs with porins immobilized onto the surface[15−18] or confined inside synthetic pores.[19−21] Specifically, although the effectiveness of NMs is regulated by the amount of porin molecules active for the ion transport, controlling their orientation once immobilized onto the surface or inside nanopores is a challenge that has not been achieved yet. However, the identification of temperature intervals, in which protein molecules experience local structural re-arrangements with an enhancement of intermolecular β-sheets, suggests that soft postthermal treatments could be very advantageous to improve the efficacy of the NMs. Thus, this could be achieved by heating the proteins from their initial assembly state to denaturalization and, subsequently, cooling under controlled conditions to maximize favorable interactions. The amount of protein molecules contributing to the selective ion transport substrate could be substantially increased by enhancing the intermolecular β-sheets, which requires local orientation of the immobilized biomolecules.

ASSOCIATED CONTENT

Supporting Information

The Supporting Information is available free of charge on the ACS Publications website at DOI: 10.1021/acsomega.8b00463.

Materials, experimental methods, and characterization data; additional FTIR and CD spectra; roughness data; and resonance and surface stress parameters (PDF)

AUTHOR INFORMATION

Corresponding Author

*E-mail: carlos.aleman@upc.edu (C.A.).

ORCID

Carlos Alemán: 0000-0003-4462-6075

Author Contributions

‖M.L.-R. and A.P.-J contributed equally to this study.

Notes

The authors declare no competing financial interest.

ACKNOWLEDGMENTS

This work was supported by MINECO (MAT2015-69367-R) and AGAUR (2017 SGR 359). M.L.-R. acknowledges the FI grant to the Generalitat of Catalunya. Support for the research of C.A. was received through the prize "ICREA Academia" for excellence in research funded by the Generalitat de Catalunya. C.M. and E.A.P. thank the Belgian National Fund for Scientific Research for their research associate and senior research associate positions, respectively. Diffraction experiments (ID-2016091886) were performed at NCD beamline (BL11-NCD) at ALBA Synchrotron (Barcelona, Spain). The authors are indebted to Prof. Jordi Puiggalí for his assistance in synchrotron experiments.

REFERENCES

(1) Tamayo, J.; Kosaka, P. M.; Ruz, J. J.; San Paulo, Á.; Calleja, M. Biosensors based on nanomechanical systems. *Chem. Soc. Rev.* **2013**, *42*, 1287−1311.

(2) Li, M.; Tang, H. X.; Roukes, M. L. Ultra-sensitive NEMS-based cantilevers for sensing, scanned probe and very high-frequency applications. *Nat. Nanotechnol.* **2007**, *2*, 114−120.

(3) Chaste, J.; Eichler, A.; Moser, J.; Ceballos, G.; Rurali, R.; Bachtold, A. A nanomechanical mass sensor with yoctogram resolution. *Nat. Nanotechnol.* **2012**, *7*, 301−304.

(4) Ndieyira, J. W.; Watari, M.; Barrera, A. D.; Zhou, D.; Vögtli, M.; Batchelor, M.; Cooper, M. A.; Strunz, T.; Horton, M. A.; Abell, C.; Rayment, T.; Aeppli, G.; McKendry, R. A. Nanomechanical detection of antibiotic-mucopeptide binding in a model for superbug drug resistance. *Nat. Nanotechnol.* **2008**, *3*, 691−696.

(5) Kosaka, P. M.; Tamayo, J.; Ruz, J. J.; Puertas, S.; Polo, E.; Grazu, V.; de la Fuente, J. M.; Calleja, M. Tackling reproducibility in microcantilever biosensors: A statistical approach for sensitive and specific end-point detection of immunoreactions. *Analyst* **2013**, *138*, 863−872.

(6) Soccio, M.; Luongo, G.; Esteves, C.; Salvador-Matar, A.; Ahumada, O.; Rueda, D. R.; García-Gutiérrez, M. C.; Lotti, N.; Munari, A.; Ezquerra, T. A. Thermomechanical response of a semicrystalline polymer in the vicinity of the melting by using microcantilever technology. *Appl. Phys. Lett.* **2014**, *104*, 251904.

(7) Ahumada, O.; Pérez-Madrigal, M. M.; Ramirez, J.; Curcó, D.; Esteves, C.; Salvador-Matar, A.; Luongo, G.; Armelin, E.; Puiggalí, J.; Alemán, C. Sensitive thermal transitions of nanoscale polymer samples using the bimetallic effect: application to ultra-thin polythiophene. *Rev. Sci. Instrum.* **2013**, *84*, 053904.

(8) Rebollar, E.; Sanz, M.; Esteves, C.; Martínez, N. F.; Ahumada, O.; Castillejo, M. Gold coating of micromechanical DNA biosensors by pulsed laser deposition. *J. Appl. Phys.* **2013**, *112*, 084330.

(9) Bumbu, G.-G.; Wolkenhauer, M.; Kircher, G.; Gutmann, J. S.; Berger, R. Micromechanical cantilever technique: A tool for investigating the swelling of polymer brushes. *Langmuir* **2007**, *23*, 2203−2207.

(10) del Rey, M.; da Silva, R. A.; Meneses, D.; Petri, D. F. S.; Tamayo, J.; Calleja, M.; Kosaka, P. M. Monitoring swelling and deswelling of thin polymer films by microcantilever sensors. *Sens. Actuators, B* **2014**, *204*, 602−610.

(11) Dominguez, C. M.; Ramos, D.; Mendieta-Moreno, J. I.; Fierro, J. L. G.; Mendieta, J.; Tamayo, J.; Calleja, M. Effect of water-DNA interactions on elastic properties of DNA self-assembled monolayers. *Sci. Rep.* **2017**, *7*, 536.

(12) Malvar, O.; Ruz, J. J.; Kosaka, P. M.; Domínguez, C. M.; Gil-Santos, E.; Calleja, M.; Tamayo, J. Mass and stiffness spectrometry of

DOI: 10.1021/acsomega.8b00463
ACS Omega 2018, 3, 7856−7867

nanoparticles and whole intact bacteria by multimode nanomechanical resonators. *Nat. Commun.* **2016**, *7*, 13452.
(13) Naik, A. K.; Hanay, M. S.; Hiebert, W. K.; Feng, X. L.; Roukes, M. L. Towards single-molecule nanomechanical mass spectrometry. *Nat. Nanotechnol.* **2009**, *4*, 445−450.
(14) Shen, Y.-X.; Saboe, P. O.; Sines, I. T.; Erbakan, M.; Kumar, M. Biomimetic membranes: A review. *J. Membr. Sci.* **2014**, *454*, 359−381.
(15) Ali, M.; Nasir, S.; Nguyen, Q. H.; Sahoo, J. K.; Tahir, M. N.; Tremel, W.; Ensinger, W. Metal Ion Affinity-based Biomolecular Recognition and Conjugation inside Synthetic Polymer Nanopores Modified with Iron-Terpyridine Complexes. *J. Am. Chem. Soc.* **2011**, *133*, 17307−17314.
(16) Hou, X.; Guo, W.; Jiang, L. Biomimetic smart nanopores and nanochannels. *Chem. Soc. Rev.* **2011**, *40*, 2385−2401.
(17) Pérez-Madrigal, M. M.; del Valle, L. J.; Armelin, E.; Michaux, C.; Roussel, G.; Perpète, E. A.; Alemán, C. Polypyrrole-supported membrane proteins for bio-inspired ion channels. *ACS Appl. Mater. Interfaces* **2015**, *7*, 1632−1643.
(18) Zhang, X.; Fu, W.; Palivan, C. G.; Meier, W. Natural channel protein inserts and functions in a completely artificial, solid-supported bilayer membrane. *Sci. Rep.* **2013**, *3*, 2196.
(19) Hall, A. R.; Scott, A.; Rotem, D.; Mehta, K. K.; Bayley, H.; Dekker, C. Hybrid pore formation by directed insertion of α-haemolysin into solid-state nanopores. *Nat. Nanotechnol.* **2010**, *5*, 874−877.
(20) Balme, S.; Janot, J.-M.; Berardo, L.; Henn, F.; Bonhenry, D.; Kraszewski, S.; Picaud, F.; Ramseyer, C. New bioinspired membrane made of a biological ion channel confined into the cylindrical nanopore of a solid-state polymer. *Nano Lett.* **2011**, *11*, 712−716.
(21) Puiggalí-Jou, A.; Pérez-Madrigal, M. M.; del Valle, L. J.; Armelin, E.; Casas, M. T.; Michaux, C.; Perpète, E. A.; Estrany, F.; Alemán, C. Confinement of a β-barrel protein in nanoperforated free-standing nanomembranes for ion transport. *Nanoscale* **2016**, *8*, 16922−16935.
(22) Roussel, G.; Matagne, A.; De Bolle, X.; Perpète, E. A.; Michaux, C. Purification, refolding and characterization of the trimeric Omp2a outer membrane porin from Brucella Melitensis. *Protein Expression Purif.* **2012**, *83*, 198−204.
(23) Roussel, G.; Perpète, E. A.; Matagne, A.; Tinti, E.; Michaux, C. Towards a universal method for protein refolding: The trimeric beta barrel membrane Omp2a as a test case. *Biotechnol. Bioeng.* **2013**, *110*, 417−423.
(24) Whitmore, L.; Wallace, B. A. Protein secondary structure analyses from circular dichroism spectroscopy: methods and reference databases. *Biopolymers* **2008**, *89*, 392−400.
(25) Lechuga Gómez, L.; Álvarez-Sanchéz, V.; Tamayo De Miguel, F. J. U.S. Patent 7,646,494 B2, 2010.
(26) Tamayo De Miguel, F. J.; Mertens, J.; Calleja-Gómez, M. U.S. Patent 7,978,344 B2, 2011.
(27) Weiss, M. S.; Palm, G. J.; Hilgenfeld, R. Crystallization, structure solution and refinement of hen egg-white lysozyme at pH 8.0 in the presence of MPD. *Acta Crystallogr., Sect. D: Biol. Crystallogr.* **2000**, *56*, 952−958.
(28) Majorek, K. A.; Porebski, P. J.; Dayal, A.; Zimmerman, M. D.; Jablonska, K.; Stewart, A. J.; Chruszcz, M.; Minor, W. Structural and immunologic characterization of bovine, horse, and rabbit serum albumins. *Mol. Immunol.* **2012**, *52*, 174−182.
(29) Murayama, K.; Tomida, M. Heat-Induced secondary structure and conformation change of bovine serum albumin investigated by fourier transform infrared spectroscopy. *Biochemistry* **2004**, *43*, 11526−11532.
(30) Meermans, F.; Atilgan, C.; Miles, A. J.; Bader, R.; Shang, W.; Matagne, A.; Wallace, B. A.; Koch, M. H. J. Consistent picture of the reversible thermal unfolding of hen egg-white lysozyme from experiment and molecular dynamics. *Biophys. J.* **2010**, *99*, 2255−2263.
(31) Knubovets, T.; Osterhout, J. J.; Connolly, P. J.; Klibanov, A. M. Structure, thermostability, and conformational flexibility of hen egg-white lysozyme dissolved in glycerol. *Proc. Natl. Acad. Sci. U.S.A.* **1999**, *96*, 1262−1267.
(32) Chen, C. R.; Makhatadze, G. I. Molecular determinants of temperature dependence of protein volume change upon unfolding. *J. Phys. Chem. B* **2017**, *121*, 8300−8310.
(33) Chalikian, T. V.; Bresalauer, K. J. On volume changes accompanying conformational transitions of biopolymers. *Biopolymers* **1996**, *39*, 619−626.
(34) Maji, S. K.; Wang, L.; Greenwald, J.; Riek, R. Structure-activity relationship of amyloid fibrils. *FEBS Lett.* **2009**, *583*, 2610−2617.
(35) Eisenberg, D. The discovery of the -helix and -sheet, the principal structural features of proteins. *Proc. Natl. Acad. Sci. U.S.A.* **2003**, *100*, 11207−11210.
(36) Martínez, N. F.; Kosaka, P. M.; Tamayo, J.; Ramírez, J.; Ahumada, O.; Mertens, J.; Hien, T. D.; Rijn, C. V.; Calleja, M. High throughput optical readout of dense arrays of nanomechanical systems for sensing applications. *Rev. Sci. Instrum.* **2010**, *81*, 125109.
(37) Puiggalí-Jou, A.; del Valle, L. J.; Alemán, C.; Pérez-Madrigal, M. M. Weighing biointeractions between fibrin(ogen) and clot-binding peptides using microcantilever sensors. *J. Pept. Sci.* **2017**, *23*, 162−171.
(38) Barnes, J. R.; Stephenson, R. J.; Woodburn, C. N.; O'Shea, S. J.; Welland, M. E.; Rayment, T.; Gimzewski, J. K.; Gerber, C. A femtojoule calorimeter using micromechanical sensors. *Rev. Sci. Instrum.* **1994**, *65*, 3793−3798.
(39) Zeth, K.; Thein, M. Porins in prokaryotes and eukaryotes: Common themes and variations. *Biochem. J.* **2010**, *431*, 13−22.
(40) Tamm, L. K.; Hong, H.; Liang, B. Folding and assembly of β-barrel membrane proteins. *Biochim. Biophys. Acta* **2004**, *1666*, 250−263.
(41) Moon, C. P.; Zaccai, N. R.; Fleming, P. J.; Gessmann, D.; Fleming, K. G. Membrane protein thermodynamic stability may serve as the energy sink for sorting in the periplasm. *Proc. Natl. Acad. Sci. U.S.A.* **2013**, *110*, 4285−4290.
(42) Kleinschmidt, J. H. Folding and stability of monomeric β-barrel membrane proteins. *Protein-Lipid Interactions*, 1st ed.; Tamm, L. K., Ed.; Wiley VCH: Weinheim, 2006; pp 27−56.
(43) Fioroni, M.; Dworeck, T.; Rodríguez-Ropero, F. β-Channels in proteins as tools in Nanotechnology. *Advances in Experimental Medicine and Biology*; Springer, 2014; Vol. *794*.
(44) Greenfield, N. J. Using circular dichroism collected as a function of temperature to determine the thermodynamics of protein unfolding and binding interactions. *Nat. Protoc.* **2007**, *1*, 2527−2535.
(45) Saha, P.; Manna, C.; Chakrabarti, J.; Ghosh, M. Reversible thermal unfolding of a yfdX protein with chaperone-like activity. *Sci. Rep.* **2016**, *6*, 29541.
(46) Sukumaran, S.; Hauser, K.; Maier, E.; Benz, R.; Mäntele, W. Structure-function correlation of outer membrane protein porin fromParacoccus denitrificans. *Biopolymers* **2006**, *82*, 344−348.
(47) Sukumaran, S.; Zscherp, C.; Mäntele, W. Investigation of the thermal stability of porin fromParacoccus denitrificansby site-directed mutagenesis and Fourier transform infrared spectroscopy. *Biopolymers* **2004**, *74*, 82−86.
(48) Solov'eva, T. F.; Likhatskaya, G. N.; Khomenko, V. A.; Stenkova, A. M.; Kim, N. Y.; Portnyagina, O. Y.; Novikova, O. D.; Trifonov, E. D.; Nurminski, E. A.; Isaeva, M. P. A Novel OmpY Porin From Yersinia Pseudotuberculosis: Structure, Channel-Forming Activity and Trimer Thermal Stability. *J. Biomol. Struct. Dyn.* **2011**, *28*, 517−533.
(49) Stoppel, W. L.; White, J. C.; Horava, S. D.; Bhatia, S. R.; Roberts, S. C. Transport of biological molecules in surfactant-alginate composite hydrogels. *Acta Biomater.* **2011**, *7*, 3988−3998.
(50) Hill, S. E.; Miti, T.; Richmond, T.; Muschol, M. Spatial extent of charge repulsion regulates assembly pathways for lysozyme amyloid fibrils. *PLoS One* **2011**, *6*, e18171.
(51) Alvarez, M.; Lechuga, L. M. Microcantilever-based platforms as biosensing tools. *Analyst* **2010**, *135*, 827−836.
(52) Hwang, K. S.; Eom, K.; Lee, J. H.; Chun, D. W.; Cha, B. H.; Yoon, D. S.; Kim, T. S.; Park, J. H. Dominant surface stress driven by biomolecular interactions in the dynamical response of nanomechanical microcantilevers. *Appl. Phys. Lett.* **2006**, *89*, 173905.

DOI: 10.1021/acsomega.8b00463
ACS Omega 2018, 3, 7856−7867

(53) Thakur, G.; Jiang, K.; Lee, D.; Prashanthi, K.; Kim, S.; Thundat, T. Investigation of pH-induced protein conformation changes by nanomechanical deflection. *Langmuir* **2014**, *30*, 2109−2116.

DOI: 10.1021/acsomega.8b00463
ACS Omega 2018, 3, 7856−7867